Temperature dependence of TiN elastic constants from *ab initio* molecular dynamics simulations

Peter Steneteg,[*] Olle Hellman, Olga Yu. Vekilova, Nina Shulumba, Ferenc Tasnádi, and Igor A. Abrikosov

Department of Physics, Chemistry and Biology (IFM), Linköping University, SE-581 83 Linköping, Sweden

Elastic properties of cubic TiN are studied theoretically in a wide temperature interval. First-principles simulations are based on *ab initio* molecular dynamics (AIMD). Computational efficiency of the method is greatly enhanced by a careful preparation of the initial state of the simulation cell that minimizes or completely removes a need for equilibration and therefore allows for parallel AIMD calculations. Elastic constants C_{11}, C_{12}, and C_{44} are calculated. A strong dependence on the temperature is predicted, with C_{11} decreasing by more than 29% at 1800 K as compared to its value obtained at $T = 0$ K. Furthermore, we analyze the effect of temperature on the elastic properties of polycrystalline TiN in terms of the bulk and shear moduli, the Young's modulus and Poisson ratio. We construct sound velocity anisotropy maps, investigate the temperature dependence of elastic anisotropy of TiN, and observe that the material becomes substantially more isotropic at high temperatures. Our results unambiguously demonstrate the importance of taking into account finite temperature effects in theoretical calculations of elastic properties of materials intended for high-temperature applications.

I. INTRODUCTION

The physical and mechanical properties of transition-metal nitrides such as chemical stability, high hardness, high melting point, and excellent electrical and thermal conductivity, make them attractive for technological applications and motivate intense research. In particular, nitrides of early transition metals, such as Ti, Cr, Hf, Zr, and their alloys with, e.g., Al and Si, represent basic building blocks for modern commercially available hard, wear-resistant coated cutting tools. It is well established that a thermal treatment, either postgrowth or upon the tool operation, strongly affects the coating film performance. For instance, one observes a formation of self-organized nanostructures[1–4] and modification of the films phase composition and microstructure at elevated temperature. The exposure of the transition-metal nitrides to high temperature and high pressure in technological applications can be either beneficial or detrimental,[5,6] underlying the importance of studies of their thermal stability, microstructure evolution, and hardness at conditions corresponding to operation conditions of cutting tools.[6–9]

Various experimental techniques are employed for this purpose.[10] Differential scanning calorimetry has been used successfully to study the thermal responses during annealing. Analytical scanning transmission electron microscopy with energy dispersive spectroscopy and x-ray diffraction (XRD) were used for microstructure characterization and nanoindentation for mechanical property determination of as-deposited and annealed coatings.[6–9] At the same time, *ab initio* computer simulations in the framework of density functional theory (DFT) have become increasingly important for the interpretation of the experimental information,[11,12] predictions of materials properties,[13–20] and for the knowledge-based materials design.[4] The accuracy and reliability of theoretical calculations have substantially increased, to the extent that in the absence of corresponding experimental information, or in cases when it is limited, computed properties have become accepted by the research community almost at the same level of trust as measured data. However, state-of-the-art DFT simulations are still most often carried out for static models, with atoms at fixed lattice positions. Even at zero temperature this is an approximation, which neglects zero-point atomic motion, and in certain cases leads to non-negligible errors for such basic properties as lattice parameters.[21] It has been demonstrated that the errors for lattice stabilities due to the neglect of temperature effects in simulations can be as large as a factor of 2.[22]

One class of properties that has attracted particular interest is the elastic behavior of transition-metal nitrides.[16–20] Indeed, it influences many important phenomena that determine the hard-coating performance. For example, TiN films display a completely elastic response at low loads.[23] Furthermore, the elastic anisotropy is essential for understanding and modeling the spinodal decomposition,[24] which occurs in some alloys of transition-metal nitrides and it is believed to be the main reason for the age hardening effect.[7,8,25] At the same time, experimental information on elastic properties of transition-metal nitrides is mostly limited to their Young's moduli.[23,26–29] With rare exceptions it does not include data on the single-crystal elastic constants.[30] Therefore, first-principles calculations are employed to obtain the missing information on elastic constants for these materials. Methodological advances[20,31,32] have made it possible to extend the study of elasticity from ordered compounds to disordered solid solutions. Still, to the best of our knowledge all available calculations of elastic properties of transition-metal nitrides are restricted to static models at zero temperature. It is generally believed that the inclusion of temperature effects cannot substantially increase the predictive quality of the calculated elastic constants, and that the increase in computational efforts is therefore not justified unless one is interested in their behavior at extreme conditions.[33,34]

One the other hand, the applied force of a cutting tool against the work piece, together with the minimal contact area, gives rise to stress and pressure levels of several GPa at the cutting edge. The temperature can often raise above 1000 K during the operation.[35] Thus, in the case of transition-metal nitrides we do deal with extreme conditions,

both in industrial applications and in simulations of their phase stability[5,13–15] and microstructure evolution.[36] In this work we demonstrate the importance of taking into account finite temperature effects in theoretical calculations of elastic properties of materials intended for hard-coating applications. We calculate elastic properties of prototypical transition-metal nitride, TiN, within a wide temperature interval, from room temperature to 1800 K. TiN is a general purpose coating for numerous applications. It is commonly used in machining ferrous materials, molding, the medical industry, as a diffusion barrier in electronic components, as a corrosion resistant material, and for decorative purposes. Besides being used on its own, it is a basic material for modern alloys for hard wear-resistant coatings on cutting tools. It has very high melting temperature 3223 K,[26] and its bulk modulus is believed to be the highest for stoichiometric compounds. However, its thermal stability is relatively low, and the hardness decreases rapidly with temperature,[6] indicating that bonds could become softer. Thus, one can expect that in this material temperature strongly affects the elastic constants, further justifying our choice of TiN as a model system for the present study.

Our first-principles simulations of the temperature dependence of TiN elasticity are based on *ab initio* molecular dynamics (AIMD).[33] Computational efficiency of the method is greatly enhanced by a careful preparation of the initial state of the simulation cell that minimizes or completely removes a need for equilibration and therefore allows for parallel AIMD calculations. We calculate bulk single-crystal elastic constants C_{11}, C_{12}, and C_{44}. Also, we analyze the effect of temperature on the elastic properties of polycrystalline TiN in terms of the bulk and shear moduli, the Young's modulus and Poisson ratio. We calculate single-crystal longitudinal and transverse sound wave velocities as a function of propagation direction, and investigate the temperature dependence of elastic anisotropy. We observe that the material becomes substantially more isotropic at high temperatures.

The paper is organized as follows. In Sec. II we give a detailed description of the methodology for the calculations of elastic constants, determination of sound velocities and their anisotropies, and parallel implementation of AIMD. We discuss our results in Sec. III, and summarize this work in Sec. IV.

II. METHOD OF CALCULATION

A. General procedure

AIMD has been applied to calculate the temperature dependent elastic constants of TiN. A grid of molecular dynamics (MD) simulations over volumes and temperatures has been set to find the equilibrium volume as a function of the temperature. Next at each temperature five different deformations have been generated, as described in Sec. II B below, and AIMD simulations have been performed. The elastic constants have been extracted from the derivative of the stress-strain curve for each temperature. Here we make a common approximation and neglect influence of entropic contributions to the free energy on the stress-strain relations.[33]

B. Elastic constants

In a cubic material using the Voigt notation the elastic constants are defined by the relation[37]

$$\sigma_i = \sum_j C_{ij}\epsilon_j, \tag{1}$$

where σ_i and ϵ_j are elements of the stress and strain tensors. Due to cubic symmetry the elastic tensor C_{ij} only has three nonvanishing, inequivalent elements C_{11}, C_{12}, and C_{44}. To obtain the elastic constants a strain tensor

$$\epsilon(\eta) = \begin{pmatrix} \eta & \eta/2 & 0 \\ \eta/2 & 0 & 0 \\ 0 & 0 & 0 \end{pmatrix} \tag{2}$$

can be used, where η is the magnitude of the distortion. By inserting it in Eq. (1) the following relations can be derived for C_{ij}:

$$\frac{d\sigma_1(T)}{d\eta} = C_{11}(T), \tag{3}$$

$$\frac{d\sigma_2(T)}{d\eta} = C_{12}(T), \tag{4}$$

$$\frac{d\sigma_6(T)}{d\eta} = C_{44}(T). \tag{5}$$

By calculating the stress σ_i for a set of deformations $\epsilon(\eta) + I$, with η deviating a few percent from zero, the derivative of σ can be found and the elastic constants extracted. To include the effect of temperature, the stresses σ are calculated for a set of time steps N_t from a molecular dynamics simulation at the specific temperature and at the equilibrium volume for that temperature. This procedure generates a set of stresses at each value of η, the distribution of which can be seen in Fig. 1. To find the derivative, a second-order polynomial is fitted to the whole set of points at each temperature using the least-square method.

Experimentally, polycrystalline materials containing many randomly oriented grains with different sizes, are often studied. In AIMD elastic constants are calculated for single crystals, but using the Reuss and the Voigt approaches one can obtain expressions for bulk (B_R, B_V) and shear (G_R, G_V) moduli for polycrystals.[37] For cubic systems the following
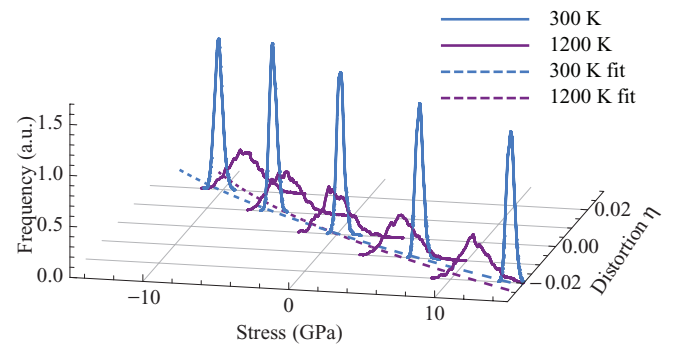

FIG. 1. (Color online) Distribution of stresses obtained by AIMD simulations at each value of distortion η and at two temperatures, 300 and 1200 K. Solid lines are histograms of all the instantaneous σ_{11} stress values. Dashed lines correspond to C_{11} strain-stress curves fitted to the stress data, from which the values of $C_{11}(T)$ are extracted.

relations exist:

$$B_R = B_V = B, \qquad (6)$$

$$B = \frac{C_{11} + 2C_{12}}{3}, \qquad (7)$$

$$G_V = \frac{C_{11} - C_{12} + 3C_{44}}{5}, \qquad (8)$$

$$G_R = \frac{5(C_{11} - C_{12})C_{44}}{3(C_{11} - C_{12}) + 4C_{44}}. \qquad (9)$$

The Young's modulus E and Poisson ratio ν can be calculated as

$$E_{V,R} = \frac{9BG_{V,R}}{3B + G_{V,R}}, \qquad (10)$$

$$\nu_{V,R} = \frac{3B - G_{V,R}}{2(3B + G_{V,R})}. \qquad (11)$$

For polycrystalline materials it is useful to define a measure of elastic anisotropy as

$$A_{V,R} = \frac{G_V - G_R}{G_V + G_R}. \qquad (12)$$

C. Sound velocities

The most general relationship between the speed of acoustic waves V in solids and its density ρ and adiabatic bulk modulus B is given by the Newton-Laplace equation

$$V = \sqrt{\frac{B}{\rho}}. \qquad (13)$$

In isotropic materials, the P- (primary, longitudinal) and S- (shear, secondary, transverse) wave velocities can be expressed with the help of thermodynamic variables,

$$V_s = \sqrt{\frac{G}{\rho}} \quad \text{and} \quad V_p = \sqrt{\frac{B + \frac{4}{3}G}{\rho}}, \qquad (14)$$

where G is the shear modulus. However, sound velocities can also be obtained from the elastic stiffness constants C_{ij}. In the general case the sound velocities in the long-wavelength limit can be derived from the Green-Christoffel equations:[38]

$$\rho \ddot{u}_\alpha = \sum_{\beta\gamma\delta} C_{\alpha\beta,\gamma\delta} \frac{\partial^2 u_\gamma}{\partial r_\delta \partial r_\beta}, \qquad (15)$$

where $\alpha\beta\gamma\delta$ are Cartesian indices, u is the displacement, and r is a Cartesian coordinate. It is solved with a plane-wave ansatz where the frequencies ω and polarization vectors $\vec{\epsilon}$ are given by

$$\tilde{C}_q \vec{\epsilon}_q = \rho \omega_q^2 \vec{\epsilon}_q, \qquad (16)$$

where

$$\tilde{C}_q^{\alpha\delta} = \sum_{\beta\gamma} C_{\alpha\gamma,\beta\delta} q_\gamma q_\delta. \qquad (17)$$

The sound velocity in direction q is then given by

$$V_q = \frac{\omega_q}{q}. \qquad (18)$$

In high-symmetry directions, when $\vec{\epsilon} \parallel q$ or $\vec{\epsilon} \perp q$, the modes are called pure longitudinal or transverse, respectively. In all other directions the wave that has the polarization vector closest to q is called quasilongitudinal (V_p), while the other two are classified as quasitransverse waves (V_{s1}, V_{s2}).

D. Parallel molecular dynamics

To speed up the calculations and achieve a representative set of uncorrelated samples we employed a parallel approach to MD. We note that when averaging stresses, one does not need consecutive time steps. Following a scheme according to West and Estreicher[39] we prepare the supercells in a thermally excited state. First we calculate the interatomic force constant matrix using the temperature dependent effective potential method of Hellman *et al.*[40] From the secular equation for the dynamical matrix we obtain the normal mode canonical transformation that diagonalizes the classical harmonic Hamiltonian. The $3N_a$ normal modes commensurate with the supercell are described by the eigenvalues ω_k^2 and eigenvectors ϵ_k (k is the mode index). The inverse of this transformation provides us with displacement u_j and velocity $\dot{u}_j$ of atom j,

$$u_j = \sum_{k=1}^{3N_a} \epsilon_{jk} c_k e^{i(\omega_k t + \delta_k)}, \qquad (19)$$

$$\dot{u}_j = \sum_{k=1}^{3N_a} i \epsilon_{jk} c_k \omega_k e^{i(\omega_k t + \delta_k)}. \qquad (20)$$

The amplitudes of the modes are defined up to the constant c_k and an unknown phase δ_k. We know that the velocity components should be normally distributed with a standard deviation of $\sigma = \sqrt{k_b T/m}$ and that each mode k should contribute, on average, $k_B T/2$ to the internal energy. By choosing the coefficients in accordance to the Box-Muller transform[41]

$$c_k = \frac{1}{\omega_k} \sqrt{\frac{k_B T}{m_j}} \sqrt{-2 \ln \chi_1}, \qquad (21)$$

$$\delta_k = 2\pi \chi_2 \qquad (22)$$

with χ_1 and χ_2 uniformly distributed on the interval $0 < \chi \leqslant 1$ these criteria are fulfilled.

Molecular dynamics initiated like this requires little to no time for equilibration, hence allowing for an embarrassingly[42] parallel high-throughput execution of AIMD, efficiently utilizing high-performance computational resources.

E. Computational details

All MD simulations in this work are carried out with the projector augmented wave method[43] as implemented in the Vienna Ab Initio Simulation Package (VASP).[44–46] The electronic exchange-correlation is modeled using the generalized gradient approximation.[47] The simulation cell consists of $4 \times 4 \times 4$ primitive TiN unit cells in total 64 Ti and 64 N atoms. 500 eV plane-wave cutoff is used to achieve accurate stresses. The Brillouin zone is sampled using the Monkhorst-Pack scheme[48] with a grid of $2 \times 2 \times 2$ k points. All the simulations use a canonical ensemble (NVT) to

maintain the desired temperature. The Nose thermostat[49] is used with the default mass value as implemented in VASP.

The elastic constants are calculated at six temperatures: 300, 600, 900, 1200, 1500, and 1800 K. For each temperature five different values of $\eta \in \{-0.02, -0.01, 0.00, 0.01, 0.02\}$ have been used for the deformation matrix $\epsilon(\eta) + I$. For each deformation five parallel molecular dynamics simulations are performed, with a total of about 20 000 time steps.

By calculating the elastic constants independently for each of the five parallel molecular dynamics simulations, a standard deviation can be extracted, making it possible to estimate the statistical errors of the method.

III. RESULTS

A. Single-crystal elastic constants

In Fig. 2 we summarize the obtained temperature variation of the elastic constants of B1 TiN. One sees that the elastic constants calculated by means of AIMD at room temperature are in good agreement with the corresponding zero-temperature values obtained with conventional static calculations. Furthermore, these later agree well with earlier *ab initio* calculations (see, for example, Ref. 50). Though we are not aware of any experimental measurements of the temperature dependence of elastic properties in this material, it is possible to show the reliability of our simulations. If it is not shown, the error is less than the symbol in the graph. In comparing our room-temperature data with experiment, it is important to underline that TiN is stable in the broad range of compositions, from $TiN_{0.6}$ to $TiN_{1.1}$,[50] and that its elastic properties depend on the degree of off-stoichiometry.[29] We observe very good agreement with the experimental measurements carried out on nearly stoichiometric TiN films grown on (001) cubic MgO substrates for C_{11}, 611 GPa (theory) and 625 GPa (experiment), as well as for C_{44} elastic
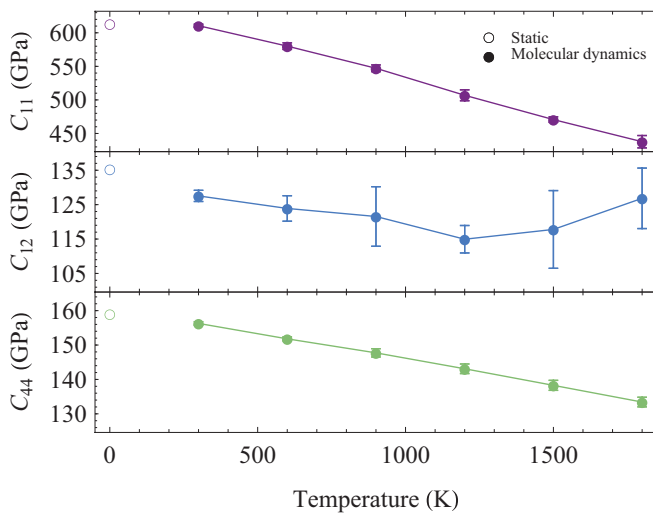

FIG. 2. (Color online) Calculated single-crystal elastic constants for B1 TiN as a function of temperature. Theoretical results obtained from AIMD simulations are shown with filled circles connected with solid lines. Static calculations at $T = 0$ K are shown with open circles. The error bars correspond to a standard deviation, calculated from the variance of five independent molecular dynamics simulations.

constants, 156 GPa and 163 GPa for theory and experiment, respectively. The difference between theory and experiment for C_{12} elastic constant is somewhat larger; 128 GPa and 165 GPa, respectively. The origin of this difference is not clear immediately. But we would like to point out that our result is in good agreement with majority of other first-principles calculations.[51] Moreover, the bulk modulus B, 320 GPa, obtained in Ref. 30 is also somewhat larger than the value obtained in most first-principles calculations, as well as in an independent experiment,[52] where it is found to be 292 GPa. The latter is in excellent agreement with our bulk modulus 289 GPa at 300 K. Considering Eq. (7) and the good agreement between theory and experiment for C_{11}, one may wish to have an independent measurement of C_{12} elastic constant in TiN, at least at room temperature.

Though the difference between calculated and measured values of C_{12} is not too big, it has important consequences for the analysis of the bonding situation and mechanical integrity in this compound. The angular character of atomic bonding in materials can be characterized by the Cauchy pressure $P_C = (C_{12} - C_{44})$,[53] a phenomenological criterion that is often used for a prediction of brittle vs ductile behavior.[54,55] For brittle materials with strong degree of directional covalent bonds, the Cauchy pressure is negative. According to our calculations, TiN should be brittle at room temperature, in agreement with experiment.[56] Note that room-temperature experimental data from Ref. 30 gives slightly positive values of the Cauchy pressure.

Thus, we conclude that our AIMD simulations give reliable results for C_{ij} at room temperature, and we can now analyze their temperature evolution. For both C_{11} and C_{44} we observe nearly linear decrease with increasing temperature, indicating normal temperature dependence, caused by anharmonicity.[37] For C_{12} there is no clear trend, and the dependence we observe is mostly within the the error bars. Indeed for many systems at temperatures below the melting temperature the dependence of elastic constants on T can be fitted to the empirical relation[57]

$$C_{ij}(T) = C_{ij}(0)(1 - bTe^{-T_0/T}), \qquad (23)$$

where b is a constant and T_0 is of the order of 1/3 of the Debye temperature θ_D. Anomalous temperature dependence is also possible, where violation of Eq. (23) can be caused by electronic structure effects. For intermediate temperatures $T_0 \ll T$ the leading terms are

$$C_{ij}(T) = C_{ij}(0)[1 - b(T - T_0)], \qquad (24)$$

showing linearity with T. Close to the melting temperature, high-order anharmonic effects should result in strong nonlinear temperature dependence.[37] As $\theta_D = 636$ K for TiN, the temperature window for our simulations fulfills the criterion $T_0 < T < T_m$, making the observed nearly linear dependence of elastic constants on temperature into another justification of the reliability of the proposed methodology.

We notice that for elastic constants C_{11} and C_{44}, a strong dependence on the temperature is predicted. C_{11} decreases with 28%, from 611 GPa to 438 GPa between room temperature and 1800 K. In this sense, the effect of temperature on elastic constants is comparable to the effect of alloying, e.g., with Al (Ref. 19) or the effect of off-stoichiometry.[29] Accordingly, the

temperature dependence of the elastic constants should not be neglected in the analysis of elastic behavior of hard materials.

B. Sound velocities and their anisotropies

As discussed in Sec. II C, calculated elastic constants allow us to analyze the propagation of sound waves in TiN. In Fig. 3 we show three-dimensional projection of the sphere of the sound velocities plotted in all directions. One sees from Figs. 3(a) and 3(d), representing the V_p velocities for the temperatures 300 K and 1500 K, respectively, a slight decrease in sound velocity, less than 10%, with increasing temperature. The directions of the maximum and minimum velocity remain unchanged, as well as the topology of the diagram. The same tendency is seen for V_{s1} and V_{s2} velocities at the considered temperatures. However, in all cases we observe a substantial, nearly factor of 2, decrease in sound wave anisotropy. For V_p the anisotropy decreases from 10.8% to 5.9%, for V_{s2} from 16.8% to 8.8%, and for V_{s1} from 24.3%

to 13.0%. We conclude that TiN becomes substantially more isotropic at high temperatures.

C. Polycrystalline elastic constants and Possion ratios

Using single-crystal elastic constants obtained in our AIMD simulations, we calculate polycrystalline elastic constants and the Poisson ratio for B1 TiN. They are displayed in Fig. 4. Similar to C_{ij}, B, E, and G show nearly linear decrease with temperature following Eq. (24). The Poisson ratio shows little temperature variation. There is good agreement between room-temperature results calculated by AIMD and zero-temperature values obtained from conventional static calculations.

Young's modulus of TiN was measured in several experiments,[23,26–30] but the data are rather scattered, ranging from 430 GPa (Ref. [29]) to 590 GPa.[26] Our calculated value of E is well within this limit. For ceramics the Poisson ratio is expected to be around 1/4,[56] which is close to our result. All polycrystalline elastic constants depend strongly on temperature, decreasing by 20%–25% between the room temperature and 1800 K. For the Young's modulus the change is very similar to the one observed by changing the N fraction in TiN from 1 to 0.66,[29] indicating that the effect of temperature on elastic properties of TiN can be as important as the effect due to off-stoichiometry. We also notice that the difference between the Reuss and the Voigt averages of the elastic constants and

(a) V_p 300 K
Min: 9.69 km/s Max: 10.7 km/s
Anisotropy: 10.8 %

(d) V_p 1500 K
Min: 9.04 km/s Max: 9.57 km/s
Anisotropy: 5.9 %

(b) V_{s1} 300 K
Min: 5.43 km/s Max: 6.75 km/s
Anisotropy: 24.3 %

(e) V_{s1} 1500 K
Min: 5.19 km/s Max: 5.86 km/s
Anisotropy: 13.0 %

(c) V_{s2} 300 K
Min: 5.43 km/s Max: 6.34 km/s
Anisotropy: 16.8 %

(f) V_{s2} 1500 K
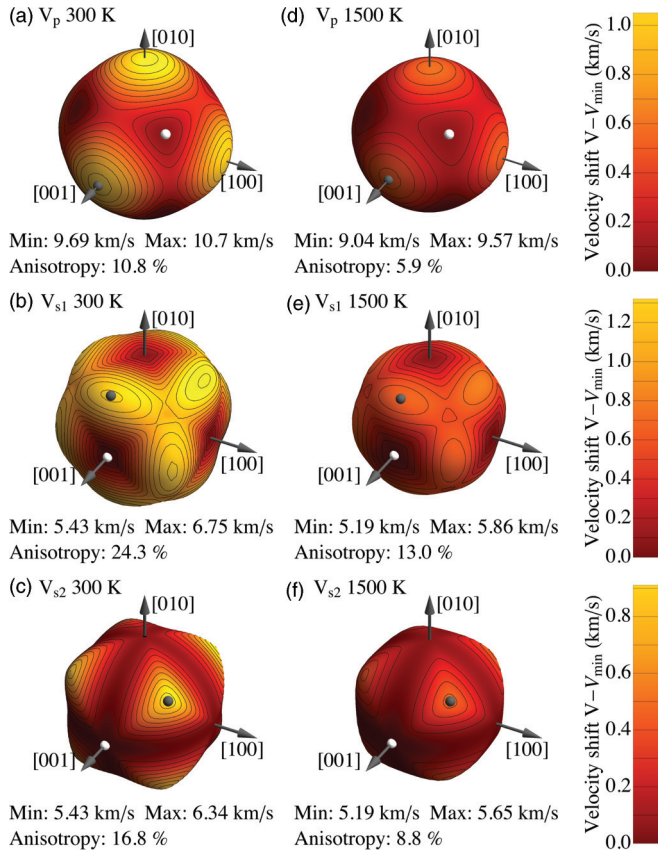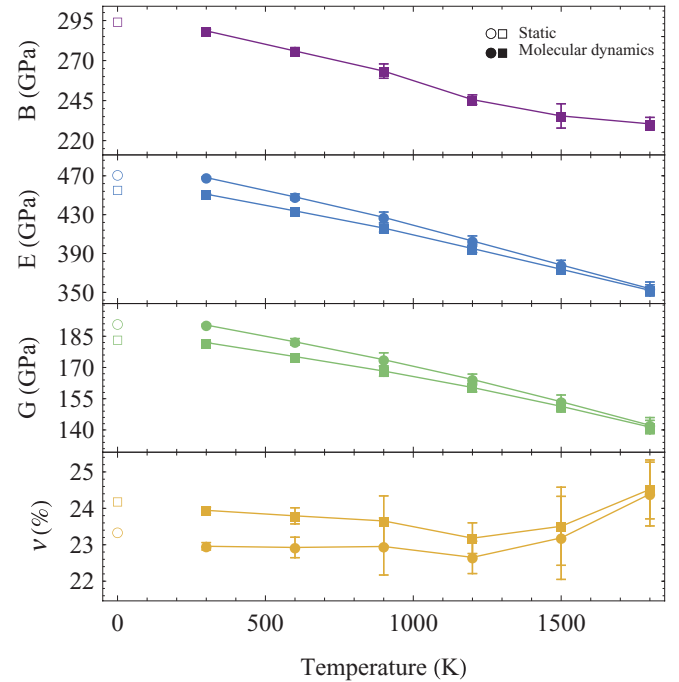Min: 5.19 km/s Max: 5.65 km/s
Anisotropy: 8.8 %

FIG. 3. (Color online) Single-crystal longitudinal and transverse sound velocities for B1 TiN at temperatures $T = 300$ K: (a) V_p, (b) V_{s1}, and (c) V_{s2} and $T = 1500$ K: (d) V_p, (e) V_{s1}, and (f) V_{s2} as a function of propagation direction. All velocities are given in (km/s). The deformed spheres show the directional dependency of the sound velocities. The radius and color are proportional to the sound velocity in the corresponding direction. The isocontours are drawn at fixed intervals for each polarization, starting from the minimum velocity at each temperature and polarization. Fewer contours correspond to a more isotropic velocity distribution. White and black spheres indicate the direction of the minimum and maximum velocity, respectively.

FIG. 4. (Color online) Calculated polycrystalline elastic constants, bulk modulus B (a), Young's modulus E (b), shear modulus G (c), as well as Poisson ratio (d) for B1 TiN as a function of temperature. The results of the averaging using the Reuss and the Voigt approaches are indicated with circles and squares, respectively. Theoretical results obtained from AIMD simulations are connected with solid lines. Static calculations at $T = 0$ K are shown with open symbols. The error bars correspond to a standard deviation, calculated from the standard deviations in C_{ij} assuming the errors are normally distributed.
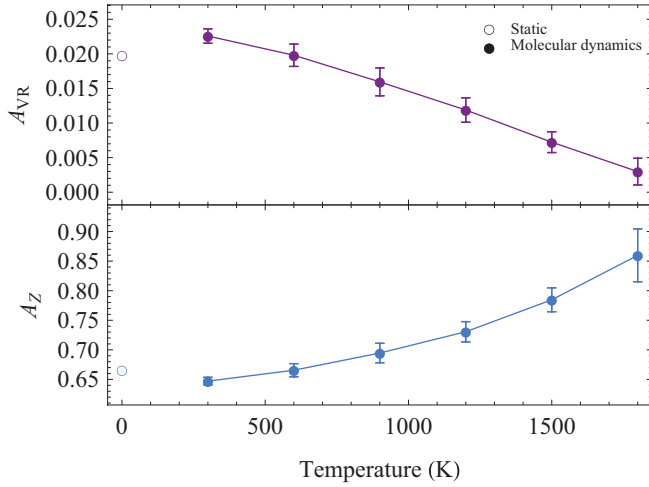
FIG. 5. (Color online) Calculated Voigt-Reuss-Hill anisotropy A_{VR} and Zenner elastic-shear anisotropy index A_Z for B1 TiN as a function of temperature. Theoretical results obtained from AIMD simulations are connected with solid lines. Static calculations at $T = 0$ K are shown with open symbols. The error bars correspond to one standard deviation, calculated from the standard deviations in C_{ij} assuming the errors are normally distributed.

the Poisson ratio decreases with temperature, pointing to a decrease in the elastic anisotropy. At room temperatures G/B value is below 0.5, indicating that TiN is a brittle material, in agreement with experiment[56] and an analysis of Cauchy pressure presented in Sec. III A.

D. Elastic anisotropy

A measure of the elastic anisotropy can be experimentally determined by the strain ratio and then recalculated into the ratio between Young's moduli E_{hkl} in different directions.[19] E_{hkl} can also be calculated from the single-crystal elastic constants.[30,37] Our AIMD simulations at room temperature give $E_{100} = 567$ GPa, $E_{110} = 429$ GPa, and $E_{111} = 397$ GPa, in good agreement with their experimental values 556, 446, and 418 GPa for $\langle 100 \rangle$, $\langle 110 \rangle$, and $\langle 111 \rangle$ directions, respectively.[30] Consequently, the calculated elastic moduli ratio at room temperature $E_{100} : E_{110} : E_{111} = 1 : 0.76 : 0.7$ is also in good agreement with experiment.[19,30]

To further quantify the temperature dependence of elastic anisotropy, we present in Fig. 5 the calculated anisotropy values defined according to Voigt-Reuss-Hill, Eq. (12), as well as according to Zener:[37]

$$A_Z = \frac{2C_{44}}{C_{11} - C_{12}}. \quad (25)$$

In isotropic materials the former approaches 0, while the latter goes to 1. Similar to the observations made from the calculation of elastic wave velocities we conclude from Fig. 5 that TiN becomes more isotropic at high temperatures. The elastic isotropy is rarely expected in compounds, but it was demonstrated in Ref. 19, both theoretically and experimentally,

that $Ti_{1-x}Al_xN$ alloy becomes isotropic at $x \approx 0.28$. One can expect that the temperature effects could modify this composition.

IV. SUMMARY AND CONCLUSIONS

We demonstrate that first-principles simulations based on AIMD allow for accurate calculations of elastic properties of materials at elevated temperature. Though the simulations are substantially more time consuming in comparison to static calculations of elastic constants, they are necessary for the proper description of elastic behavior at extreme conditions, which are likely to be present in many modern technological processes. We show that computational efficiency of the AIMD method can be greatly enhanced by a careful preparation of the initial state of the simulation cell that minimizes or completely removes the need for equilibration. Therefore it allows for a parallel implementation of the calculations, and substantially reducing the execution times for the project.

We study elastic properties of a prototypical transition-metal nitride TiN between room temperature and 1800 K, which corresponds to operational conditions for cutting tool coatings. We calculate principal cubic elastic constants C_{11}, C_{12}, and C_{44}, as well as the polycrystalline elastic constants bulk B and shear moduli G, and Young's modulus E and Poisson ratio ν. The elastic constants decrease nearly linearly with increasing temperature, indicating normal temperature dependence, caused by anharmonicity. We observe particularly strong dependence on the temperature for C_{11} that decreases by 28% between room temperature and 1800 K. Also, B, G, and E decrease by 20%–to 25% in this temperature interval. The effect of temperature on elastic behavior of TiN is, thus, as strong as the effect of alloying with Al or N off-stoichiometry. We construct sound velocity anisotropy maps and investigate the temperature dependence of elastic waves and elastic constants anisotropy of TiN. We predict that the material becomes substantially more isotropic at high temperatures. Our results unambiguously demonstrate the importance of taking into account finite temperature effects in theoretical calculations of elastic properties of materials intended for high-temperature applications.

---

[1]S. Veprek, J. Nanosci. Nanotechnol. **11**, 14 (2011).

[2]A. Flink, J. Andersson, B. Alling, R. Daniel, J. Sjölén, L. Karlsson, and L. Hultman, Thin Solid Films **517**, 714 (2008).

[3] P. H. Mayrhofer, C. Mitterer, L. Hultman, and H. Clemens, Prog. Mater. Sci. **51**, 1032 (2006).

[4] H. Lind, R. Forsen, B. Alling, N. Ghafoor, F. Tasnadi, M. P. Johansson, I. A. Abrikosov, and M. Oden, Appl. Phys. Lett. **99**, 091903 (2011).

[5] B. Alling, M. Oden, L. Hultman, and I. A. Abrikosov, Appl. Phys. Lett. **95**, 181906 (2009).

[6] A. Knutsson, M. P. Johansson, L. Karlsson, and M. Oden, J. Appl. Phys. **108**, 044312 (2010).

[7] A. Horling, L. Hultman, M. Oden, J. Sjolen, and L. Karlsson, J. Vac. Sci. Technol. A **20**, 1815 (2002).

[8] A. Hörling, L. Hultman, M. Odén, J. Sjölén, and L. Karlsson, Surf. Coat. Technol. **191**, 384 (2005).

[9] R. Rachbauer, S. Massl, E. Stergar, D. Holec, D. Kiener, J. Keckes, J. Patscheider, M. Stiefel, H. Leitner, and P. H. Mayrhofer, J. Appl. Phys. **110**, 023515 (2011).

[10] I. A. Abrikosov, A. Knutsson, B. Alling, F. Tasnádi, H. Lind, L. Hultman, and M. Odén, Materials **4**, 1599 (2011).

[11] R. F. Zhang, A. S. Argon, and S. Veprek, Phys. Rev. Lett. **102**, 015503 (2009).

[12] T. Marten, B. Alling, E. I. Isaev, H. Lind, F. Tasnádi, L. Hultman, and I. A. Abrikosov, Phys. Rev. B **85**, 104106 (2012).

[13] P. H. Mayrhofer, D. Music, and J. M. Schneider, Appl. Phys. Lett. **88**, 071922 (2006).

[14] B. Alling, A. V. Ruban, A. Karimi, O. E. Peil, S. I. Simak, L. Hultman, and I. A. Abrikosov, Phys. Rev. B **75**, 045123 (2007).

[15] B. Alling, A. V. Ruban, A. Karimi, L. Hultman, and I. A. Abrikosov, Phys. Rev. B **83**, 104203 (2011).

[16] K. Chen, L. R. Zhao, J. Rodgers, and J. S. Tse, J. Phys. D **36**, 2725 (2003).

[17] R. Kato and J. Hama, J. Phys.: Condens. Matter **6**, 7617 (1994).

[18] P. H. Mayrhofer, D. Music, and J. M. Schneider, J. Appl. Phys. **100**, 094906 (2006).

[19] F. Tasnádi, I. A. Abrikosov, L. Rogstrom, J. Almer, M. P. Johansson, and M. Oden, Appl. Phys. Lett. **97**, 231902 (2010).

[20] F. Tasnádi, M. Odén, and I. A. Abrikosov, Phys. Rev. B **85**, 144112 (2012).

[21] E. I. Isaev, S. I. Simak, A. S. Mikhaylushkin, Y. K. Vekilov, E. Y. Zarechnaya, L. Dubrovinsky, N. Dubrovinskaia, M. Merlini, M. Hanfland, and I. A. Abrikosov, Phys. Rev. B **83**, 132106 (2011).

[22] C. Asker, A. B. Belonoshko, A. S. Mikhaylushkin, and I. A. Abrikosov, Phys. Rev. B **77**, 220102 (2008).

[23] H. Ljungcrantz, M. Oden, L. Hultman, J. E. Greene, and J.-E. Sundgren, J. Appl. Phys. **80**, 6725 (1996).

[24] D. Seol, S. Hu, Y. Li, J. Shen, K. Oh, and L. Chen, Acta Mater. **51**, 5173 (2003).

[25] P. H. Mayrhofer, A. Horling, L. Karlsson, J. Sjolen, T. Larsson, C. Mitterer, and L. Hultman, Appl. Phys. Lett. **83**, 2049 (2003).

[26] H. Holleck, J. Vac. Sci. Technol. A **4**, 2661 (1986).

[27] M. E. O'Hern, R. H. Parrish, and W. C. Oliver, Thin Solid Films **181**, 357 (1989).

[28] D. S. Stone, J. Vac. Sci. Technol. A **9**, 2543 (1991).

[29] D.-J. Shu, S.-T. Ge, M. Wang, and N.-B. Ming, Phys. Rev. Lett. **101**, 116102 (2008).

[30] J. O. Kim, J. D. Achenbach, P. B. Mirkarimi, M. Shinn, and S. A. Barnett, J. Appl. Phys. **72**, 1805 (1992).

[31] L. Vitos, I. A. Abrikosov, and B. Johansson, Phys. Rev. Lett. **87**, 156401 (2001).

[32] J. von Pezold, A. Dick, M. Friák, and J. Neugebauer, Phys. Rev. B **81**, 094203 (2010).

[33] L. Vočadlo, Earth Planet. Sci. Lett. **254**, 227 (2007).

[34] O. Gülseren and R. E. Cohen, Phys. Rev. B **65**, 064103 (2002).

[35] R. M'saoubi and S. Ruppi, CIRP Ann. **58**, 57 (2009).

[36] L. Rogström, J. Ullbrand, J. Almer, L. Hultman, B. Jansson, and M. Odén, Thin Solid Films **520**, 5542 (2012).

[37] G. Grimvall, *Thermophysical Properties of Materials*, 1st ed. (Elsevier, New York, 1999).

[38] G. Srivastava, *The Physics of Phonons* (A. Hilger, Bristol, UK, 1990).

[39] D. West and S. K. Estreicher, Phys. Rev. Lett. **96**, 115504 (2006).

[40] O. Hellman, I. A. Abrikosov, and S. I. Simak, Phys. Rev. B **84**, 180301 (2011).

[41] G. E. P. Box and M. E. Muller, Ann. Math. Statist. **29**, 610 (1958).

[42] I. Foster, *Designing and Building Parallel Programs: Concepts and Tools for Parallel Software Engineering*, 1st ed. (Addison Wesley, Reading, MA, 1995).

[43] P. E. Blöchl, Phys. Rev. B **50**, 17953 (1994).

[44] G. Kresse and J. Hafner, Phys. Rev. B **48**, 13115 (1993).

[45] G. Kresse and J. Furthmüller, Phys. Rev. B **54**, 11169 (1996).

[46] G. Kresse and J. Furthmuller, Comput. Mater. Sci. **6**, 15 (1996).

[47] J. P. Perdew, K. Burke, and M. Ernzerhof, Phys. Rev. Lett. **77**, 3865 (1996).

[48] H. J. Monkhorst and J. D. Pack, Phys. Rev. B **13**, 5188 (1976).

[49] S. Nosé, Prog. Theor. Phys. Suppl. **103**, 1 (1991).

[50] H. O. Pierson, *Handbook of Refractory Carbides and Nitrides: Properties, Characteristics, Processing, and Applications*, Materials Science and Process Technology Series (Noyes Publications, Park Ridge, NJ, 1996).

[51] Y.-M. Kim and B.-J. Lee, Acta Mater. **56**, 3481 (2008).

[52] R. A. Andrievskii and I. I. Spivak, *Prochnost tugoplavkikh soedinenii i materialov na ikh osnove* (Metallurgiia Cheliabinskoe otdelenie, 1989).

[53] D. G. Pettifor, Mater. Sci. Technol. **8** (1992).

[54] D. G. Sangiovanni, V. Chirita, and L. Hultman, Phys. Rev. B **81**, 104107 (2010).

[55] A. V. Ponomareva, E. I. Isaev, Y. K. Vekilov, and I. A. Abrikosov, Phys. Rev. B **85**, 144117 (2012).

[56] G. N. Greaves, A. L. Greer, R. S. Lakes, and T. Rouxel, Nature Mater. **10**, 986 (2011).

[57] The equation was first presented for Young's modulus of a few oxides by J. Wachtman, W. Tefft, D. Lam, and C. Apstein, Phys. Rev. **122**, 1754 (1961). But according to Ref. 37 it should be valid for many materials and other elastic constants as well.